

APPLICATION OF ACTIVE MATERIALS TO AQUATIC BIOMIMETICS

A Senior Thesis

By

Tomoka Mashio

1996-97 University Undergraduate Research Fellow

Texas A&M University

Group: ENGINEERING

Application of Active Materials to Aquatic Biomimetics

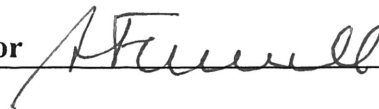
**Tomoka Mashio
University Undergraduate Fellow, 1996-1977
Texas A&M University
Department of Aerospace Engineering**

APPROVED

Fellows Advisor



Honors Director



Abstract

In the area of underwater vehicle design, the development of highly maneuverable vehicles is presently of interest with their design being based on the swimming techniques and anatomic structures of fish; primarily the undulatory body motions, the highly controllable fins and the large aspect ratio lunatic tail. The tailoring and implementation of the accumulated knowledge into biomimetic vehicles is a task of multidisciplinary nature with two of the dominant fields being actuation and hydrodynamic control.

This project is the first experimental step towards the development of a type of biomimetic muscle that utilizes Shape Memory Alloy (SMA) technology. The "muscle", which imitates the fish-like movements, is presently applied to the control of hydrodynamic forces and moments, including thrust generation, on a 2-D hydrofoil. The main actuation elements are two sets of thin SMA wires (0.015" to 0.027") embedded into an elastomeric element of the muscle that provides the main structural support. Controlled heating and cooling of the two wire sets generates bi-directional bending of the elastomer, which in turn deflects (for quasi-static control) or oscillates (for thrust generation) the trailing edge of the hydrofoil. The aquatic environment of the hydrofoil lends itself to cooling schemes that utilize the excellent heat transfer properties of water.

The modeling of deflected shapes as a function of input current has been carried out by members of Shape Memory Alloy Research Team (SMART) in the department using a thermomechanical constitutive model for SMA coupled with the elastic response of the elastomer. An approximate structural analysis model, as well as detailed FEM analysis has been performed and the model predictions have been compared with preliminary experimental measurements.

Introduction

Motivation

In aerodynamics and hydrodynamics, bird flight and fish swimming have inspired and guided the development of aircraft and underwater vehicles. It is interesting, however, to note how primitive these man-made machines seem compared to their natural counterparts in terms of intelligence, efficiency, agility, adaptiveness and functional complexity. These and other similar observations and issues have been addressed by the scientific community, and have triggered the formulation of the science of biomimetics and have inspired new approaches to old problems. The idea of aquatic biomimetics is that the state-of-the-art underwater maneuvering could be advanced by understanding and imitating the movement of fish swimming.

Previous Studies of Fish Motion

The study of fish motion dates back to work by Lighthill (1960) who applied the slender body theory of hydrodynamics to transverse oscillatory motions of slender fish, resulting in the Elongated Body Theory (EBT). This study revealed the high propulsive efficiency of fish, a finding that alone renders the utilization of similar propulsive techniques in man-made vehicles a very attractive quest. To pursue this idea, several studies have been conducted on the effect of fin appendages, the dynamics of slender fish, and the propulsion mechanisms of fish motion (Lighthill, 1960, 1970, Newman and Wu, 1973, Karpouzian et al., 1990). The propulsive investigations largely concentrated on the undulatory type of propulsion. Studies included analyses on a slender wing with passive chordwise flexibility (Katz and Weihs, 1978), 2-D potential flow modeling over a thin waving plate of finite chord (Wu, 1961, 1971, Siekmann, 1962, 1963), and 2-D flow modeling of flow over a waving plate of finite thickness (Uldrick and

Siekmann, 1964). 3-D models have more recently been developed (Cheng et al., 1991) utilizing waving plate theory, as well as comparisons of performance coefficients between fish and underwater vehicles (Bandyopadhyay et. al. 1995).

Researchers have addressed the problem of the thrust-producing capability of moving hydrofoils (Isshiki and Murakami, 1984, Koochesfahani, 1989, Triantafyllou et. al., 1991, Triantafyllou et. al., 1993, Gopalkrishnan et. al. 1994, Nakahima and Ono, 1995). This problem simulates the type of propulsion used by fish, which primarily involves the caudal, or tail, fin. The caudal fin of such animals produces thrust as it oscillates through the development of a reverse Karman vortex street that corresponds to a jet-like average velocity profile. However, such jets are convectively unstable and there is only a narrow bandwidth of frequencies for which the Karman vortices and the jet-like profile co-existence and the flow is stable (Triantafyllou et. al., 1993). For frequencies in this bandwidth, optimal thrust efficiency is achieved.

Water-Tunnel Experimental Setup

Figure 1 presents a schematic of the water-tunnel experimental rig that has been recently completed. The setup is installed in the 2'x3' Aerospace Engineering Free-Surface Water Tunnel. The effective test section is limited to 12 inches by two sheets of plexiglass to create the 2-D environment for the hydrofoil. The two vertical rails restrict the hydrofoil motion to two degrees of freedom; vertical translation and rotational motion about the pivot axis, y . For thrust/drag measurements two Omega LCL Series (LCL-005) load cells are installed at the pivot points of the hydrofoil. The attitude of the hydrofoil, i.e., plunge position, $h(t)$, angle of attack, $\alpha(t)$ and their rates of change, is fully determined through the following instrumentation: (a) a Celesco stringpot

with a 2.5' maximum travel and (b) a U.S. Digital optical encoder with 4,096 counts per revolution.

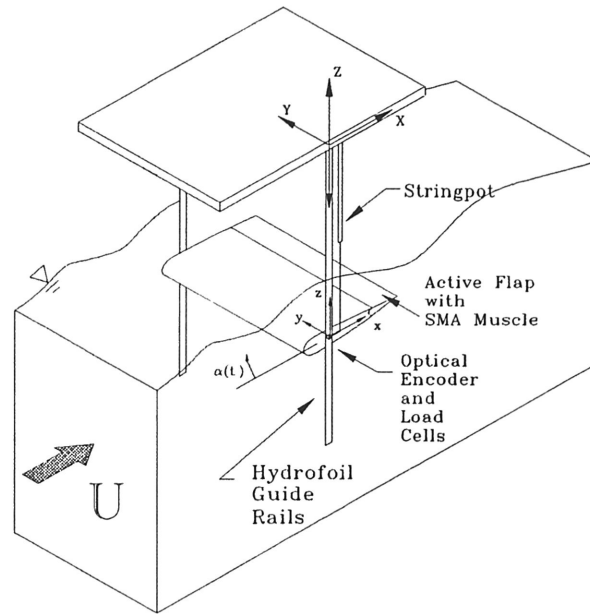


Figure 1. Water-tunnel experimental setup of the actively controlled hydrofoil

Hydrofoil Design and Initial Implementation

Full Size Water-Tunnel Model

As shown in figure 2, the hydrofoil consists three major parts; a solid main body, an SMA muscle, and a solid tip. The cross sectional shape of the hydrofoil is based on NACA 0012 except that the elastic part of SMA muscle, discussed in the following paragraph, is elongated slightly. The cross sections of solid parts in front and aft of the elastic part of the SMA muscle are 75% and 12.5% of NACA 0012 with a 15-inch chord length respectively. The elastic part of SMA

muscle has the approximate chord length of 2.5 inches. The chord length of the whole hydrofoil is 15.5 inches and the span is 12 inches.

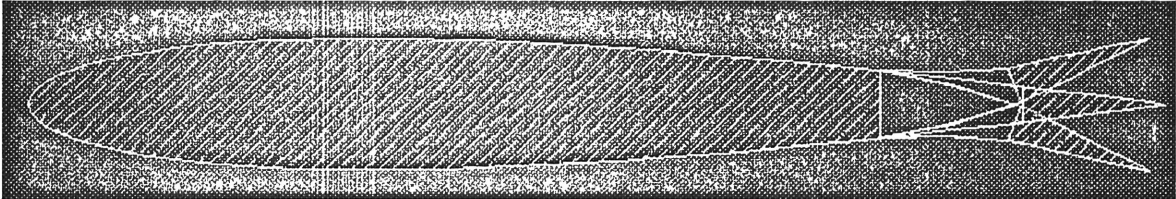


Figure 2. The SMA muscle (non-crosshatched section) can deflect or oscillate the hydrofoil's trailing edge.

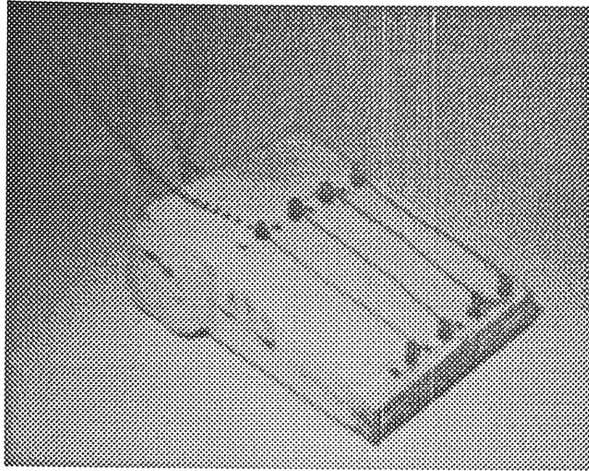
The SMA muscle includes an elastic part for a continuous bending deformation with a smooth curvature and two solid pieces for attachment to the main body and the tip. The SMA muscle is designed so that it can be detached from the hydrofoil main body and replaced with a new SMA muscle if necessary. The SMA muscle cannot be detached easily from the tip.

Shape control is achieved by embedding two sets of small-diameter SMA wires into the elastic part of the SMA muscle, one set being close to the upper surface and the other being close to the lower surface. Each surface has 12 wires, which are electrically connected in a combination of series and parallel arrangements.

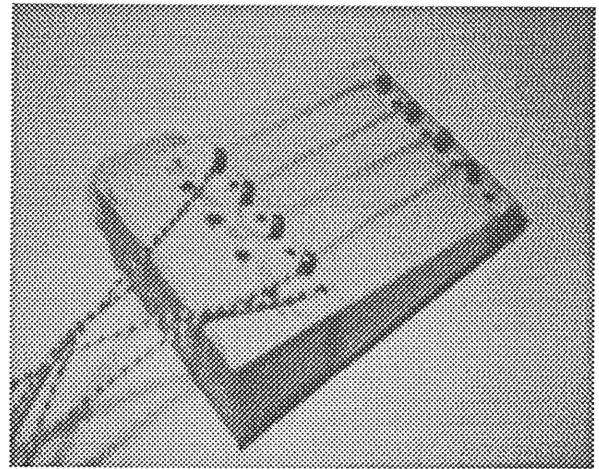
Since the temperature to activate the SMA wires reaches 100°C , a heat resistant moldable elastic material was sought to construct the SMA muscle. The silicone rubber elastomer with the durometer value of 20 meets this criteria. The frequency response of the actuation depends on the distance of the embedded wires from the surface of the elastomer because the elastomer is a good thermal insulator. In the present design, the SMA wires are not embedded in the elastomer in order to explore the maximum attainable actuation frequency. In this case a thin elastic electrically insulating coating covers each wire.

Initial Implementations

Figure 3 presents the first implementation of the actuation scheme applied to a 2.5-inch wide SMA muscle model. As seen there, the wires were positioned very close to the elastomer surface but were totally exposed to water. One can distinguish the four SMA wires running longitudinally on the upper (fig. 3a) and lower (fig. 3b) surfaces. The SMA wires were two-way trained to 3.5% strain and had a diameter of 0.015". At this stage the muscle was not instrumented with temperature or deflection sensors. Preliminary tests on the device's actuation bandwidth were encouraging. The device was submerged in a water tunnel. A 20 Amp, 20 Volt, DC power supply was used as the power source. It provided the power necessary for the resistive heating of the wires and the martensite-to-austenite phase transformation. The austenite-to-martensite phase transformation was achieved by interrupting resistive heating, and allowing the water to conduct or convect the heat off the wires, thus cooling them down to their martensitic phase temperature. Conduction (water tunnel off) and convection (water tunnel on, water velocity variable up to 1ft/sec) tests were conducted. Continuous periodic actuation frequencies as high as 1.5Hz (full transformation cycles) were achieved. However, for water velocities larger than 1ft/sec, the specific power supply was unable to heat the wires up sufficiently due to the voltage limitations. Therefore, martensite-to-austenite phase transformation was not possible.



(a)



(b)

Figure 3. Preliminary implementation of an SMA muscle.

These encouraging preliminary tests were capitalized on in the continuation of the work. A similar 4" long (chordwise dimension), 2.5" wide (spanwise dimension) SMA muscle was fabricated and fully instrumented for detailed quantitative tests. Instrumentation included:

- Two flex sensors, embedded inside the elastomer, calibrated to provide deflection feedback, one sensor for each bending direction.
- Two thermocouples attached to the two SMA wire sets, to provide wire temperature measurement and feedback.

Figure 4 presents a schematic of the instrumented muscle and the interface hardware. The data acquisition was performed by a National Instruments 16-bit A/D board. One differential input accounted for cold junction compensation, two differential inputs received the thermocouple signals and two differential inputs received the flex sensor signals. Two digital output lines (parallel port) were used to control heating of the SMA wires. Experimental data were acquired by periodically actuating the device, and will be presented at a later section along with the numerical predictions.

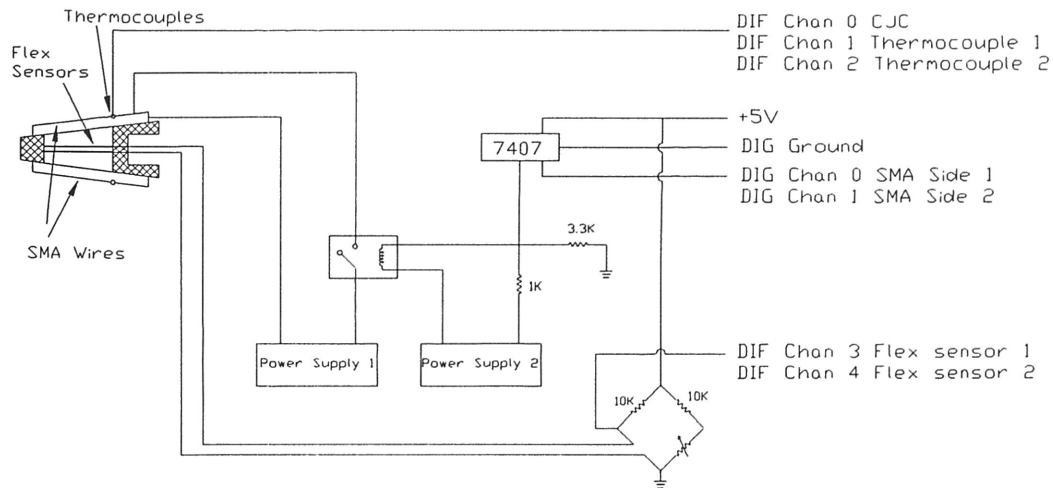


Figure 4. Schematic of SMA muscle instrumentation.

Active Materials and Shape Memory Alloys

In actuator technology, active or “smart” materials have opened up new horizons in terms of actuation simplicity, compactness and miniaturization potential. The distinct property of active materials is that they can recover the original shape after they have been deformed. Piezoelectric materials, Shape Memory Alloys (SMA) and Magnetostrictive materials are the three most recognized types. These materials most commonly develop strains or, more applicably, displacements when exposed to electric, thermal and magnetic fields respectively. Only SMA actuation is considered in this project. The high-frequency-response capabilities of piezoceramic and magnetostrictive materials (in the KHz range), are not required in this application. Also the low driving voltages to actuate SMAs are attractive because the required power driving hardware can be very simple. Nitinol (NiTi) SMAs can be actuated with very low voltages of 10 to 20V. In contrast, piezoceramic materials typically require voltages on the order of 100V for their actuation. Moreover, piezoelectric and magnetostrictive materials are only capable of producing small strains/displacements (small fractions of 1%) compared to those attained by SMA materials.

However SMA actuation is not free of drawbacks. Some of them, such as actuation loss and fatigue over repetitive cyclic loading, are in the frontier of SMA research, while others, such as low energy efficiency, are less intensely focused upon.

SMA develops strains/displacements when exposed to thermal field. Then it undergoes a change in crystal structure from a parent cubic austenitic phase to a number of martensitic variants either upon cooling or application of stress (Tanaka 1986). When it cools down, the original shape is self-recovered if the SMA is trained to be two-way (contract and expand). Otherwise the SMA needs to be pulled back to the original shape (one-way). The strain can be up to 7% for one-way trained and 4% for two-way trained SMAs.

The SMA wires employed in the SMA muscle were trained in an automated, constant-stress SMA training/modeling station developed by Shape Memory Alloy Research Team (SMART) in Aerospace Engineering Department at Texas A&M University. The device performs repeated martensite-to-austenite (M to A) and austenite-to-martensite (A to M) SMA transformation cycles and collects time records of SMA strain/displacement, load and temperature during each cycle. From the data, the SMA transformation behavior as well as behavior deterioration with the number of transformation cycles are modeled by the research team.

As it is known, rapid cooling directly affects the rate of response of the actuator. The higher the achieved heat transfer rates, the higher the achievable actuation or oscillation bandwidth. Furthermore, actuation frequency response can be improved by employing partial actuation. This can be achieved by employing partial transformation cycles. Preliminary tests of minor loops, or partial transformation loops, for a 2-way trained wire have been performed by the research team and are shown in figures 5 and 6. These tests show the shape of the hysteresis curves for minor loops with partial austenite to complete martensite transformations and vice

versa. Figure 5 shows minor loops inside a major loop, or a full transformation loop, for a constant stress test with partial austenitic transformation on the heating cycle with complete transformation to martensite upon cooling. Figure 6 shows minor loops with partial martensite transformation on the cooling cycle with complete austenitic transformation upon heating.

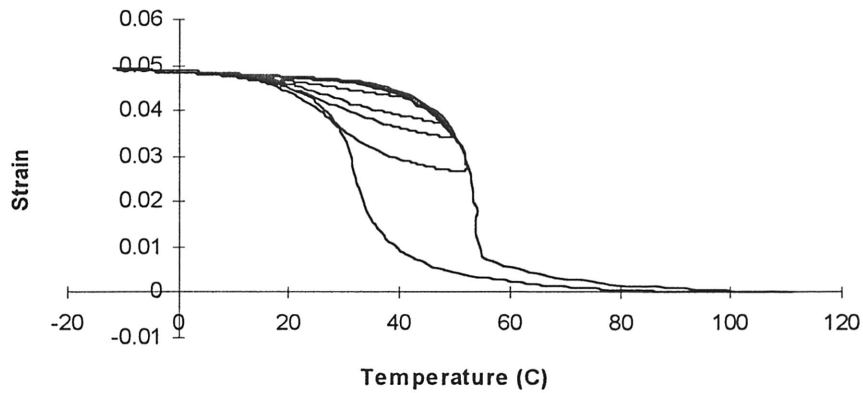


Figure 5. Strain vs. Temperature for a 2-way wire with partial austenite transformation from a fully martensitic state.

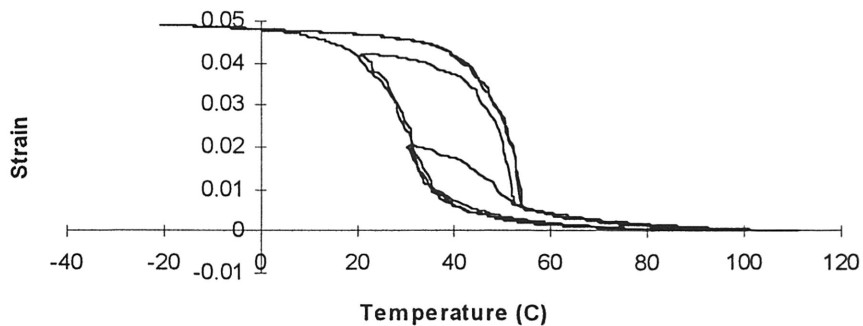


Figure 6. Strain vs. Temperature for a 2-way wire with partial martensitic transformation from a fully austenitic state.

Result and Discussion

Preliminary comparisons between experiments and numerical predictions were carried out for the case of cyclic actuation of one side of the SMA muscle, in air. The measured SMA wire temperature is shown in figure 7 for several actuation cycles. Each cycle consisted of heating the wires from 40° C to 100° C, then, by interrupting resistive heating, letting them cool down to 40° C. An approximation of the measured temperature history for one cycle (third cycle of figure 7) was used in the numerical model to predict the device's deflections, while the flex sensors provided the experimental deflections.

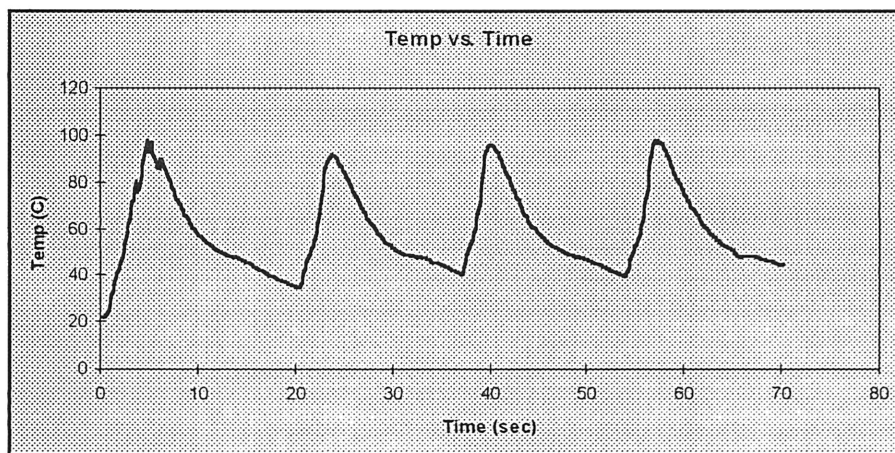


Figure 7. SMA temperature during cyclic actuation of SMA muscle in air.

In figure 8, the results from the FEM analysis are shown when the SMA wires, attached at the top surface, are actuated. The input to the SMA wires is an electric current, which induces the martensitic to austenitic phase transformation through Joule heating, while the water flow induces cooling through heat convection from the surface of the SMA wires. For a net increase in temperature above, the austenite starting temperature, A^s , the formation of austenite causes the

actuator to contract, which in turn deforms the elastomeric cross-section. The load transfer between the SMA actuators and the elastomeric material occurs through the pin joints, located at one end of the elastomer. The other end of the elastomer is assumed to be built-in, as it is attached to a much stiffer substrate. Note that the modeling of the SMA actuating wires is carried out with 1-D elements, while the elastomer is modeled with 3-D brick elements (Fig. 9).

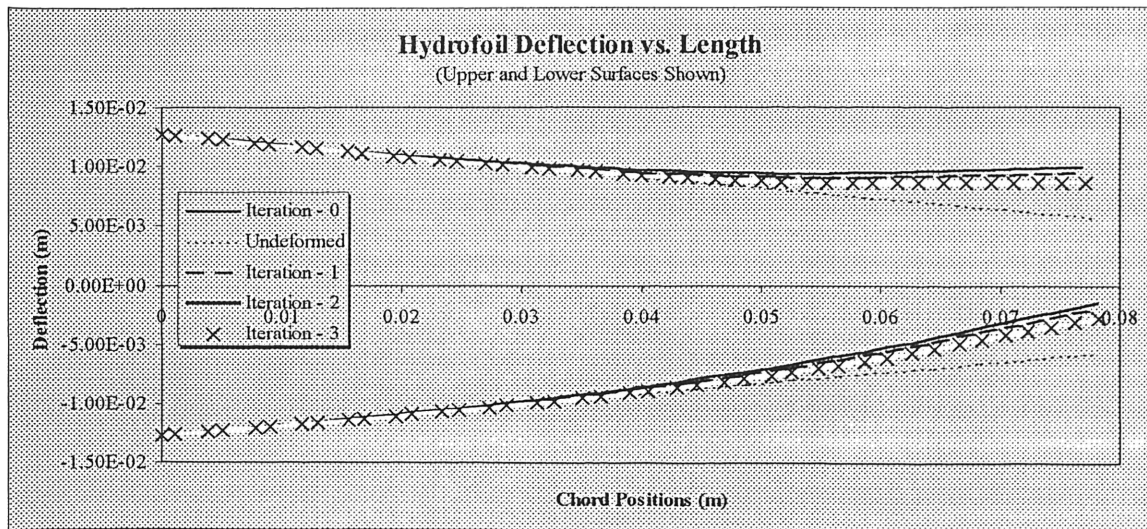


Figure 8. SMA muscle undeformed and actuated states

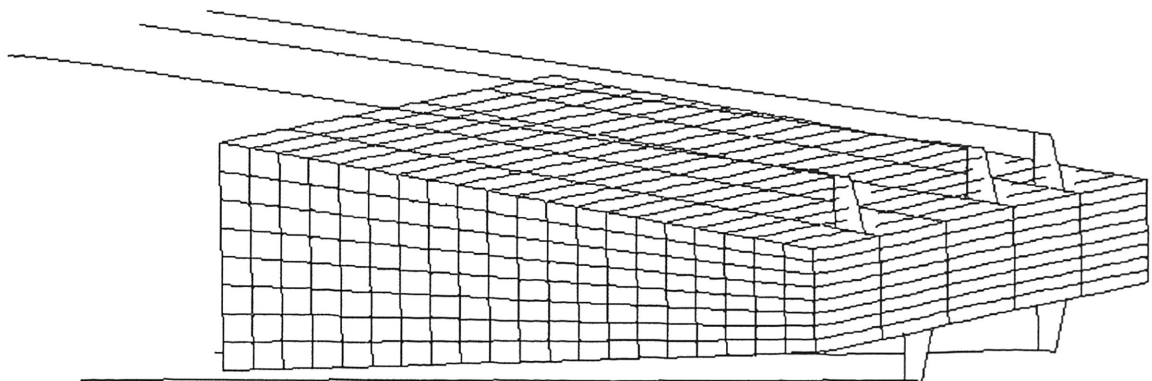


Figure 9. FEM model of the SMA muscle.

Figure 10 presents the comparison between the experimental and theoretical results. Although several features of the actuation history are identified by both experiment and simulation, it should be noted that this is only preliminary data and should be consulted more for qualitative information in the future experiments. One of the reasons for the discrepancies between predicted and measured tip rotations is the existence of “slack” in the wires of the experimental setup, which was not modeled in the numerics.

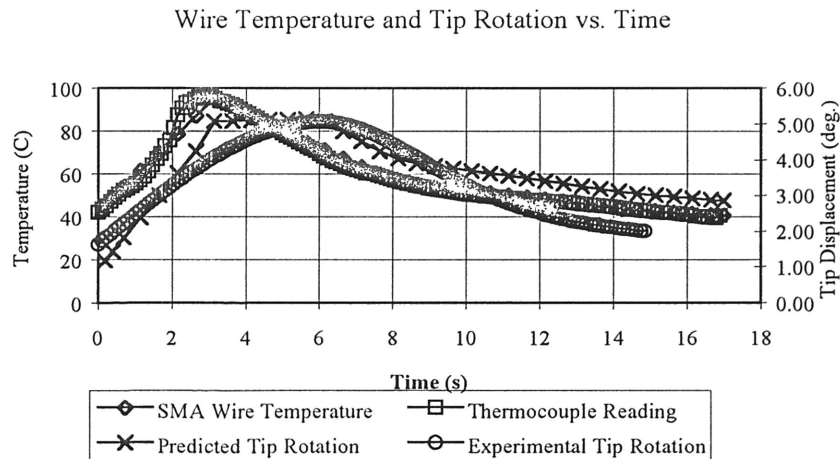


Figure 10. Wire temperature and tip rotation history during one actuation cycle.

Summary

These theoretical and experimental investigations are the first step towards the integration of hydrodynamics, active material actuation and system identification and control into a self-propelled and self-controlled hydrofoil. A biomimetic muscle that utilizes Shape Memory Alloy (SMA) technology was developed for application to the control of hydrodynamic forces and moments, including thrust generation, on a 2-D hydrofoil. The main actuation elements of the

device are two sets of thin SMA wires used to induce bending of the elastomeric element of the muscle. Controlled heating and cooling of the two wire sets generates bi-directional bending of the elastomer, which in turn deflects or oscillates the trailing edge of the hydrofoil. Preliminary tests on the device's frequency response have been performed and the results have met the expectations.

The infrastructure necessary for the study of the coupled thermomechanical/fluid-structure-interaction problem has been developed in terms of experimental setups. The integrated implementation of the iterative scheme and the comparison with experimental results is yet to be completed. An automated parameter identification procedure from experimental measurements of deflected shapes of the hydrofoil and temperature histories of SMA actuators will also be pursued next.

Bibliography

Bandyopadhyay, P.R., Rice, J.Q., Corriveau, P.J. and Macy, W.K., 1995, "Maneuvering Hydrodynamics of Fish and small Underwater Vehicles, Including the Concept of an Agile Underwater Vehicle", Naval Undersea Warfare Center Division, NUWC-NPT Technical Report 10,494.

Cheng, J.Y., Zhuang, L.X. and Tong, B.G., 1991, "Analysis of Swimming Three-Dimensional Waving Plates", *Journal of Fluid Mechanics*, Vol. 232, pp. 341-355.

Gopalkrishnan, R., Triantafyllou, M.S., Triantafyllou, G.S. and Barrett, D., "Active Vorticity Control in a Shear Flow using a Flapping Foil," *Journal of Fluid Mechanics*, Vol. 274, pp. 1-21, 1994.

Isshiki, H. and Murakami, M., 1984, "A theory of wave devouring propulsion," *Society of Naval Architects of Japan* 156, pp. 102-114.

- Karpouzian, G., Spedding G., and Cheng, H.K., 1990, "Lunate-Tail Swimming Propulsion, Part 2. Performance Analysis.", *Journal of Fluid Mechanics*, Vol. 210, No. 4, pp. 329-351.
- Katz, J. and Weihs, 1978, "Hydrodynamic Propulsion by Large Amplitude Oscillation of an Airfoil with Chordwise Flexibility", *Journal of Fluid Mechanics*, Vol. 88, No. 3, pp. 485-497.
- Lighthill, M.J., 1960, "Note on the Swimming of Slender Fish", *Journal of Fluid Mechanics*, Vol. 9, pp. 305-317.
- Lighthill, M.J., 1970, "Acquatic Animal Propulsion of High Hydrodynamical Efficiency", *Journal of Fluid Mechanics*, Vol. 44, No. 2, pp. 265-301.
- Nakashima, M. and Ono, K., 1995, "Numerical and Experimental Study of the Propulsive Speed of the Three Joint Bending Propulsion Mechanism", Tokoyo Institute of Technology, College of Engineering .
- Newman, J.M. and Wu, T.Y., 1973, "A generalized Slender Body Theory for Fish-Like Forms", *Journal of fluid Mechanics*, vol. 57, No. 4, pp. 673-693.
- Siekman, J., 1962, "Theoretical Studies of Sea Animal Locomotion, Part I", *Ingenieur-Archiv*, Vol. 31, pp214-228.
- Siekman, J., 1963, "Theoretical Studies of Sea Animal Locomotion, Part 2", *Ingenieur-Archiv*, vol. 32, pp. 40-50.
- Tanaka, K., "A Thermomechanical Sketch of Shape Memory Effect: One-Dimensional Tensile Behavior," *Res Mechanica*, Vol. 18, pp.251-263, 1986.
- Triantafyllou, G.S., Triantafyllou, M.S. and Gopalkrishnan, R., 1991, "Wake mechanics for thrust generation in oscillating foils," *Physics of Fluids A3*, pp. 2835-2837.
- Triantafyllou, G.S., Triantafyllou, M.S. and Grosenbaugh, M.A., "Optimal Thrust Development in Oscillating Foils with Application to Fish Propulsion," *Journal of Fluids and Structures*, Vol. 7, pp. 205-224, 1993.
- Uldrick, J.P. and Siekman, J., 1964, "On the Swimming of A Flexible Plate of Arbitrary Finite Thickness", *Journal of Fluid Mechanics*, Vol. 20, pp. 1-33.
- Wu, T.Y., 1961, "Swimming of a Waving Plate", *Journal of Fluid Mechanics*, Vol. 10, pp. 321-344.
- Wu, T.Y., 1971, "Hydromechanics of Swimming Propulsion, Part 1. Swimming of a Two-Dimensional Flexible Plate at Variable Forward Speeds in an Inviscid Fluid", *Journal of Fluid Mechanics*, Vol. 46, No. 2, pp. 337-355.

Wu, T.Y., 1971, "Hydromechanics of Swimming Propulsion, Part 2. Some Optimum Shape Problem", Journal of Fluid Mechanics, Vol. 46, No. 3, pp. 521-544.

Wu, T.Y., 1971, "Hydromechanics of Swimming Propulsion, Part 3. Swimming and Optimum Movements of Slender Fish with Side Fins", Journal of Fluid Mechanics, Vol. 46, No. 3, pp. 545-568.